Giant reversible magnetocaloric effect in a multiferroic $GdFeO_3$ single crystal

M. Das, S. Roy, and P. Mandal
Saha Institute of Nuclear Physics, HBNI, 1/AF Bidhannagar, Calcutta 700064, India
(Received 2 June 2017; revised manuscript received 29 September 2017; published 6 November 2017)

The magnetocaloric properties of single crystalline $GdFeO_3$ have been investigated in the temperature range 2–36 K by magnetization and heat-capacity measurements. Remarkably large and reversible magnetic entropy change, $\Delta S_m = -52.5$ J/kg K, has been observed for a field change of 0–9 T. The adiabatic temperature change, ΔT_{ad}, is also found to be very large, 22 K, slightly above the antiferromagnetic ordering temperature ($T_N^{Gd} = 2.5$ K) of the Gd^{3+} moment, for a field change of 0–8 T. These magnetocaloric parameters remain large down to the lowest temperature measured and are significantly larger than that reported for the other members of rare-earth (R) orthoferrites ($RFeO_3$) and several potential magnetic refrigerants in the same temperature range. Both ΔS_m and ΔT_{ad} are also quite large for a small field change. The large values of magnetocaloric parameters suggest that $GdFeO_3$ could be considered as a potential refrigerant in low-temperature magnetic refrigeration technology, such as liquefaction of hydrogen in the fuel industry. Moreover, $GdFeO_3$ has very low electrical conductivity and exhibits no thermal and field hysteresis in magnetization, fulfilling the necessary conditions for a good magnetic refrigerant.

DOI: 10.1103/PhysRevB.96.174405

I. INTRODUCTION

In recent times, energy-efficient and environmentally friendly technologies have received considerable attention in order to combat the problems related to the global warming and energy crisis phenomena. Magnetic-field-driven refrigeration, in which a solid material instead of environmentally harmful chlorofluorocarbon gas is used as a refrigerant, is one such emerging area in research and development. Scientists and engineers are engaged in exploring this technology to replace the conventional vapor compression technology [1–19]. Magnetic refrigeration occurs due to the change in magnetic entropy (ΔS_m) by exposing the material to a varying magnetic field. The field-induced entropy change eventually leads to a change in temperature (ΔT_{ad}) in an adiabatic condition. Thus, for any practical application, magnetic refrigeration requires a sufficiently large value of ΔS_m. For this reason, the rare-earth elements and their alloys and compounds with large total angular momentum quantum number, such as Gd, $Gd_5Si_2Ge_2$, and RAl_2 (R being rare-earth elements) [7–12], have received considerable attention. However, a large magnetocaloric effect (MCE) has also been observed in several Mn-based alloys and compounds and in Fe_2P- and LaFeSi-type systems [3,13–19], which do not contain any rare-earth elements. Primarily, the investigation of the MCE has been focused on searching for new materials that exhibit large entropy and adiabatic temperature change close to room temperature for domestic and industrial applications [1–6]. On the contrary, magnetic refrigeration in the low-temperature region has been much less focused.

Low-temperature magnetic refrigeration also has several important applications, such as in cryogenic technology in space science, for the liquefaction and storage of hydrogen in the fuel industry, and to achieve subkelvin temperatures in the laboratory for basic research. Several rare-earth transition-metal oxides and intermetallic compounds have become attractive candidates for low-temperature magnetic refrigeration [20–26]. In these materials, the rare-earth magnetic moment orders antiferromagnetically at low temperature. With the application of magnetic field, the antiferromagnetic (AFM) transition (T_N) is suppressed along with a considerable decrease in magnetic entropy in the vicinity of T_N. However, the value of magnetic entropy change decreases rapidly at low temperature. As a result, ΔS_m becomes very small just a few kelvin below the transition temperature. This is one of the major problems for the refrigeration at low temperature using a magnetically ordered material. In the recent past, it has been shown that several rare-earth transition-metal-based frustrated magnetic systems such as $RMnO_3$, $HoMn_2O_5$, etc., exhibit large MCE at low temperature [26–28]. However, both ΔS_m and ΔT_{ad} show a strong decrease below the ordering temperature of the rare-earth moment.

The $RFeO_3$-type system has received considerable attention because it exhibits several complex and interesting phenomena such as spin-flop transition, spin-reorientation transition, multiferroicity, and anisotropic magnetocaloric effect associated with the three different types of intriguing magnetic interactions R–R, R-Fe, and Fe-Fe [23,24,29–36]. However, there are very few reports on magnetic and structural properties of $GdFeO_3$ [37–39]. The details of isothermal magnetization up to high magnetic field, the field dependence of compensation temperature, and the magnetocaloric effect in $GdFeO_3$ have not been studied so far. In the present work, we have successfully grown a high-quality single crystal of $GdFeO_3$ using the floating zone technique and investigated its magnetic and magnetocaloric properties. We have chosen $GdFeO_3$ as a refrigerant material mainly due to the large angular momentum of the localized $4f$ shell electrons of Gd^{3+} ($J = 7/2$). Apart from this, in $GdFeO_3$, magnetization shows no thermal and field hysteresis and the electrical conductivity is very low, which prevents eddy current loss in the presence of magnetic field. Besides the large magnetic entropy change, the frequency of the refrigeration cycle is another important parameter for the magnetic cooling. Although $GdFeO_3$ is insulating, it shows good thermal conductivity due to the lattice contribution which helps for faster heat exchange during the refrigeration cycle [40].

In $GdFeO_3$, the Fe spin orders antiferromagnetically around $T_N^{Fe} \sim 678$ K and the nonlinear canted G-type AFM ordering of the Fe sublattice gives rise to a weak ferromagnetism

due to the Dzyaloshinskii-Moriya (DM) interaction [41]. The Gd moments also order antiferromagnetically but at a relatively low temperature, 2.5 K [41,42]. Due to the antisymmetric nature of the DM interaction, the Fe^{3+} spins order antiferromagnetically along the crystallographic a axis and the Gd^{3+} spins order along the b axis [29,43]. Our study reveals that both ΔS_m and ΔT_{ad} are very large over a wide temperature range and ΔS_m is almost temperature independent below 5 K. This behavior of $GdFeO_3$ is very different from that observed in several magnetically ordered systems and rare-earth orthoferrites [20–24]. The values of the magnetocaloric parameters are also quite large for low or moderate field strength. The role of magnetocrystalline anisotropy in magnetic and magnetocaloric properties of the $RFeO_3$ system are discussed.

II. EXPERIMENTAL DETAILS

The polycrystalline $GdFeO_3$ sample was prepared by conventional solid-state reaction method using high-purity Gd_2O_3 (99.9%) and Fe_2O_3 (99.9%) powder. Before use, Gd_2O_3 was heated at 900°C for 12 h to remove any adsorbed water and CO_2. The well-mixed powder of Gd_2O_3 and Fe_2O_3 in a stoichiometric ratio of 1:1 was heated at 1150°C for a few days with intermediate grindings. The polycrystalline $GdFeO_3$ sample was then reground and pressed into two rods of 6 mm diameter under hydrostatic pressure. Finally, the rods were sintered at 1400°C for 24 h in air. The single crystal of $GdFeO_3$ was grown in a four-mirror image furnace (Crystal Systems Inc.). The image furnace is equipped with four halogen incandescent lamps and hemielliptic focusing mirrors. Special attention was paid to achieve oxygen stoichiometry close to 3. For this reason, the crystal was grown in an oxygen atmosphere with a typical growth rate of 4 mm/h. During the growth, the feed and seed rods were rotated in opposite directions at a speed of 25 rpm.

The phase purity and the crystal structure of $GdFeO_3$ have been determined by high-resolution x-ray powder diffraction with Cu K_α radiation (Rigaku TTRAX II) ($\lambda = 1.5406\mathring{A}$) at room temperature. For the structural analysis, the Rietveld refinement of the diffraction pattern of the powdered $GdFeO_3$ single crystal was done using the FULLPROF software. The experimental x-ray intensity profile and the theoretical fit along with the Bragg positions are shown in Fig. 1. All the peaks in the diffraction pattern can be indexed well with the distorted orthorhombic unit cell having $Pbnm$ crystallographic symmetry. Within the x-ray resolution, we did not observe any peak due to the impurity phase. The lattice parameters determined from the Rietveld profile analysis are $\mathbf{a} = 5.3460$, $\mathbf{b} = 5.5879$, and $\mathbf{c} = 7.6680\mathring{A}$, which are very close to the previously reported values [39,41]. We have also characterized the sample by the Laue diffraction technique and observed very sharp Laue diffraction spots. This suggests good crystalline quality of the studied sample. The crystallographic structure of $GdFeO_3$ is shown in Fig. 2(a) and the approximate magnetic structure is shown in Fig. 2(b). The Gd^{3+} spins order along the orthorhombic **b** axis. Though the direction of Fe^{3+} spin alignment is the **a** axis, a small zero-field moment is expected along the longest **c** axis due to the DM interaction. The complexity in spin structure due to the DM interaction has not been portrayed in the figure. The details of the spin orientation are discussed in the Results and Discussion section.

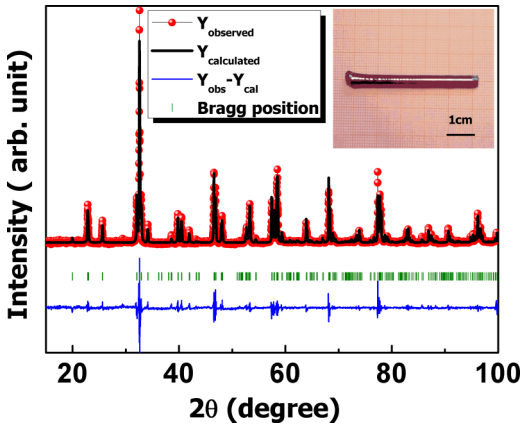

FIG. 1. The x-ray diffraction pattern of the powdered single crystal of $GdFeO_3$ grown in a floating zone image furnace. The inset shows the optical image of the crystal.

A small piece of single crystal was used for the heat capacity (C_p) measurements, which were performed in a physical property measurement system (Quantum Design). Magnetic measurements were done both in the physical property measurement system and a SQUID vibrating sample magnetometer (Quantum Design). To minimize the demagnetization effect, we have used a long parallelepiped sample and the field was applied along the longer dimension, which is the **c** axis. Data have been recorded for the isothermal dc magnetization measurement with field up to 9 T at different temperatures between 2 and 36 K, and the temperature dependence of magnetization was measured in the range 2–300 K. The heat capacity has been measured by the relaxation technique at different applied fields (0–8 T) along the **c** axis.

III. RESULTS AND DISCUSSION

The magnetization of the $GdFeO_3$ single crystal has been measured as a function of temperature under field-cooled condition with field along the **c** axis. The main panel of Fig. 3 shows $M(T)$ curves for two applied fields, 100 and 500 Oe, as representatives. The expanded view of the $M(T)$

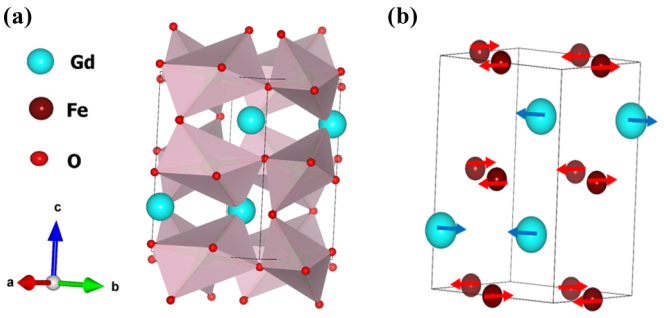

FIG. 2. (a) The orthorhombic crystal structure and (b) the magnetic structure of the $GdFeO_3$ single crystal below the antiferromagnetic ordering temperature of Gd. The arrows represent the directions of magnetic moment of Gd and Fe.

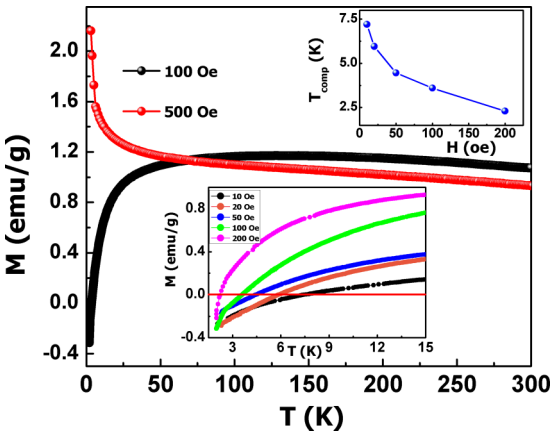

FIG. 3. Temperature dependence of the field-cooled magnetization for the $GdFeO_3$ single crystal at 100 and 500 Oe. The lower inset shows the variation of magnetization in the low-temperature regime for fields below 500 Oe and the upper inset shows the magnetic field dependence of the compensation temperature.

curves in the low-temperature region is shown in the inset of Fig. 3 for different applied fields below 500 Oe. It is clear from the figure that the nature of the $M(T)$ curve at low field is very complex due to the strong competition between the $3d$ moment of Fe^{3+} and the $4f$ moment of Gd^{3+} [41,44]. Below T_N^{Fe}, the Fe spin shows a canted G-type AFM ordering, due to the antisymmetric nature of the DM exchange interaction between the Fe moments, which prefers interacting spins to align themselves perpendicular to each other. As a result, a weak ferromagneticlike component is observed at low temperature below T_N^{Fe}. Furthermore, the antisymmetric exchange interaction or the pseudodipolar interaction between the Gd and Fe moments produces an effective magnetic field at the Gd^{3+} site, whose direction is opposite to the canted Fe^{3+} moment. This internal field (H_I) is attributed to the higher-order anisotropic exchange interaction [41]. One can see that M becomes negative at low temperature for applied field $H \leqslant 200$ Oe. The temperature, T_{comp}, below which M becomes negative is sensitive to the field strength. T_{comp} decreases from 7.3 to 2.2 K as the strength of the field increases from 10 to 200 Oe. At around T_{comp}, the moments of the two sublattices become equal in magnitude but opposite in direction; as a result, the net resultant moment is very close to zero. This is known as the compensation temperature [41]. Below T_{comp}, the net magnetic moment aligns in the opposite direction to the applied magnetic field and hence M becomes negative. At higher temperature well above T_{comp}, where the Fe^{3+} moment dominates over the Gd^{3+} moment, M is positive and decreases very slowly with increasing temperature. Several features reflected in the low-field $M(T)$ curves progressively weaken with increasing field strength and disappear above a certain field. For example, M at $H = 500$ Oe is positive, increases monotonically with decrease in T, and shows no anomalous behavior in the measured temperature range 2–300 K. From the plot of T_{comp} versus H, we have estimated the value of the critical field as $H_c \sim 350$ Oe, above which the sign-reversal phenomenon disappears. It may be noted that this value of H_c is very close to the internal magnetic field produced by the Fe^{3+} sublattice at the Gd^{3+} site [41,44]. The magnetization-reversal phenomenon has also been observed in other orthoferrites ($RFeO_3$) and in several AFM perovskites such as orthochromites, orthovanadates, and manganites [29,30,45–48]. T_{comp} for $GdFeO_3$ is comparable to that reported for $NdFeO_3$ orthoferrite [29]. On the other hand, T_{comp} and H_I are as high as 130 K and 5.5 kOe, respectively, for $GdCrO_3$ [49].

In order to understand the evolution of magnetization in the $GdFeO_3$ single crystal with the application of magnetic field, we have measured the isothermal magnetization up to 9 T at different temperatures. The magnetic field dependence of magnetization along the **c** axis is shown in Fig. 4(a) for some selected temperatures. It is clear from Fig. 4(a) that, even at low field, M increases monotonically with the decrease in T as in the case of a typical ferromagnet. This behavior of M is very different from the expected field-induced metamagnetic transition in a simple antiferromagnet. Usually, for AFM systems, M exhibits nonmonotonic temperature dependence in the low-temperature and low-field region [20–23]. At 2 K and 9 T, the value of magnetic moment is about $7.2\mu_B$/Gd, which is 3% higher than the spin-only moment of Gd ($7\mu_B$/Gd). This indicates some contribution from the Fe sublattice. The smooth evolution of M with H indicates that the field-induced transition is second order in nature. To determine the exact nature of the field-induced magnetic phase transition, the $M(H)$ curves have been transformed into the well-known Arrott plots. Figure 4(b) shows plots of M^2 versus H/M for the $GdFeO_3$ single crystal. The slope of the M^2 versus H/M curve is useful to determine the order of both temperature- and field-driven magnetic phase transition. The negative slope of the Arrott plot often indicates a first-order nature of the transition, while the positive slope implies a second-order transition. The positive slope of the M^2 versus H/M curves suggests that the field-induced phase transition in the $GdFeO_3$ single crystal is second-order continuous in nature.

Field-dependent magnetization along different crystallographic directions has been investigated in single crystals of several $RFeO_3$ (R = Dy, Er, Tb, Ho, Tm) compounds [20–24]. In all the cases, M shows strong anisotropy. Both the value of M and the nature of the $M(H)$ curve are extremely sensitive to the direction of the applied field. For example, the values of M for $DyFeO_3$ at 2 K and 7 T are $4.4\mu_B$/Dy, $7.8\mu_B$/Dy, and $0.8\mu_B$/Dy along the **a**, **b**, and **c** axes, respectively, which correspond to only 44%, 78%, and 8% of the expected moment of Dy^{3+} [20]. Also, the nature of the $M(H)$ curve changes dramatically with the field direction. Along the easy axis, M increases abruptly and tends to saturate at a relatively small applied field, while for the hard axis M increases almost linearly with field. We have also measured M with field along the **a** and **b** axes in $GdFeO_3$. In all three crystallographic directions, the value of M at 9 T and 2 K is large and close to the expected moment for the Gd^{3+} ion, and the H dependence of M is found to be very similar to what is shown in Fig. 4(a). This suggests that the field response of M in $GdFeO_3$ is very different from that reported for other orthoferrites. The observed differences in magnetic properties of $GdFeO_3$ and other orthoferrites are due to the magnetocrystalline anisotropy, which arises from the spin configuration of the R ion. Gd^{3+} is unique among the rare-earth

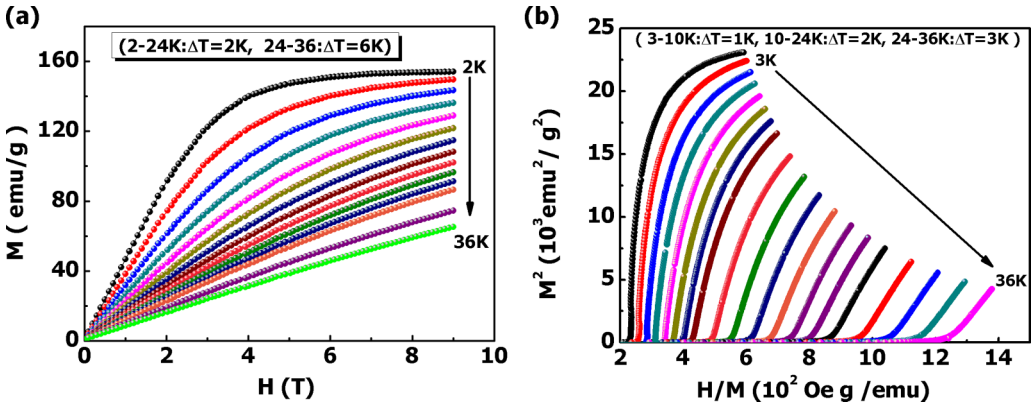

FIG. 4. (a) Some representative isothermal magnetization plots for the $GdFeO_3$ single crystal in the temperature range of 2–36 K and (b) the Arrott plots for the $GdFeO_3$ single crystal.

elements. The Gd^{3+} ion has no orbital angular momentum ($L = 0$) contribution to the total angular momentum (J). Only spin angular momentum ($S = 7/2$) contributes to J. So, the crystal field effect, which is responsible for magnetocrystalline anisotropy, is negligible in the $GdFeO_3$ compound and, as a result, magnetization is expected to be almost isotropic and large [50,51]. Due to the spin configuration of the R^{3+} ion, there is another important difference in the magnetic property of $GdFeO_3$ and other orthoferrites. $RFeO_3$ with a magnetic R ion shows a spin-reorientation transition with decreasing temperature [52]. During this process, the net moment of Fe^{3+} switches over from the **c** axis to the **a** axis, except for R = Dy, where a Morin transition occurs at around 50 K [52–54]. On the other hand, for the nonmagnetic R ion such as Lu, Y, and La, the spin-reorientation transition is absent. In $GdFeO_3$ too, the spin-reorientation transition has not been observed.

The large field-induced magnetization in the $GdFeO_3$ single crystal gives an indication of giant magnetic entropy change. To test whether this material is suitable for magnetic refrigeration, we have calculated the magnetic entropy change using the Maxwell equation, $\Delta S_m = \int_0^H (dM/dT)dH$. As the magnetization measurements are done at discrete field and temperature intervals, ΔS_m is numerically calculated using the following expression:

$$\Delta S_m = \sum_i \frac{M_{i+1} - M_i}{T_{i+1} - T_i} \Delta H_i, \qquad (1)$$

where M_i and M_{i+1} are the magnetic moments at temperatures T_i and T_{i+1}, respectively, for a small change in magnetic field ΔH_i. The temperature dependence of ΔS_m has been deduced from the magnetic field dependence of the magnetization at different temperatures using the above relation. Figure 5(a) presents the temperature dependence of ΔS_m for the field variation up to 9 T. It is very clear from the figure that ΔS_m is very large and negative down to the lowest measured temperature. The maximum value of ΔS_m (ΔS_m^{max}) increases with the increase in field and reaches as high as 52.5 J/kg K for the field change of 0–9 T, which is more than double the reported values of ΔS_m for other members of the orthoferrite series [20–24]. This difference in magnetocaloric properties arises mainly due to the magnetocrystalline anisotropy of the rare-earth ions. We would also like to mention that the observed value of ΔS_m is significantly larger than that reported for several rare-earth transition-metal oxides and intermetallic compounds [13–16]. Apart from the value, the nature of temperature dependence of ΔS_m is also very important for application in low-temperature refrigeration. We have already mentioned that ΔS_m in a typical ferromagnet or antiferromagnet shows a sharp decrease at low temperature due to the onset of long-range magnetic ordering. For examples, the Gd sublattice in $GdVO_4$ and $RuSr_2GdCu_2O_8$ also orders antiferromagnetically at 2.5 K but ΔS_m in these systems decreases rapidly below 5 K and becomes very small

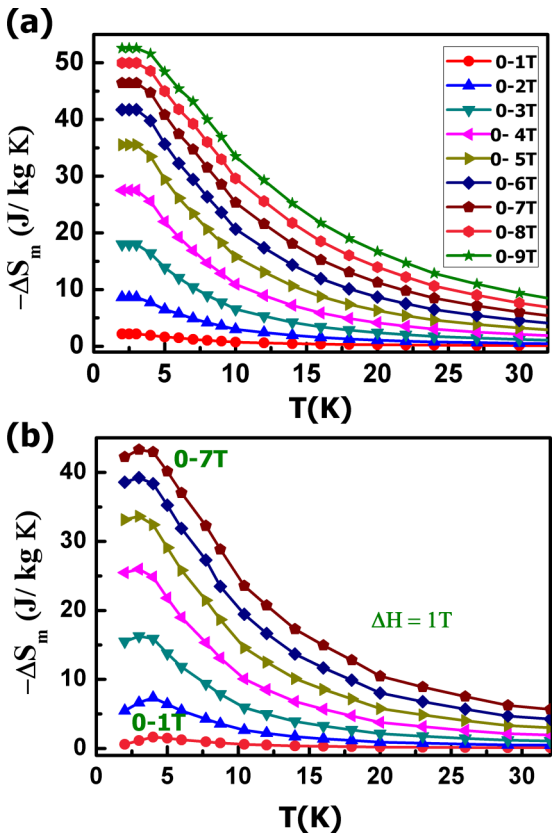

FIG. 5. Temperature variation of ΔS_m calculated from the magnetization data for $GdFeO_3$: (a) single crystal and (b) polycrystalline sample.

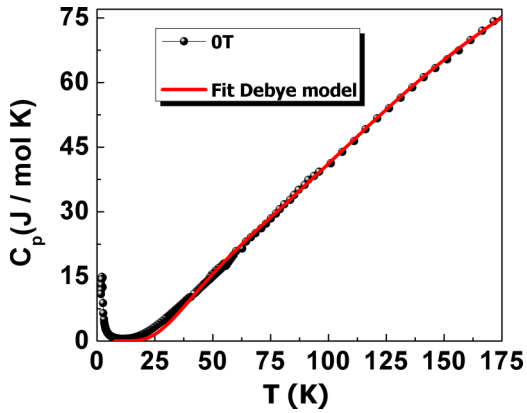

FIG. 6. Temperature dependence of the zero-field heat capacity. The solid line is the Debye model fit to the experimental data of the $GdFeO_3$ single crystal.

and even changes its sign [55,56]. On the other hand, in the present system, ΔS_m does not show any decrease down to 2 K, but a saturationlike behavior appears below 5 K. For application, ΔS_m should have a reasonably large value at low or moderate magnetic field strength. From Fig. 5, one can see that ΔS_m is quite large even at low field. For example, the values of ΔS_m^{max} are 9 and 18 J/kg K for the field changes of 2 and 3 T, respectively, which can be achieved using a permanent magnet.

From the application point of view, it is important to investigate the magnetocaloric properties of the polycrystalline sample. The temperature dependence of ΔS_m is shown in Fig. 5(b) for the $GdFeO_3$ polycrystalline sample. The value of ΔS_m for the polycrystalline sample is also very large. ΔS_m^{max} is 44 J/kg K at 7 T, which is about 4% smaller than the corresponding value at 7 T for the single crystal. However, the nature of the $\Delta S_m(T)$ curve for the polycrystalline sample is slightly different. With the decrease in temperature, ΔS_m increases down to ~3K and then decreases. Though ΔS_m decreases at low temperature, the decrease is very slow compared to several other low-temperature magnetic refrigerants, including orthoferrites. This suggests polycrystalline $GdFeO_3$ can also be considered for magnetic refrigeration. Though the observed giant MCE in $GdFeO_3$ is mainly due to the high moment of Gd^{3+}, a much weaker crystal field effect also plays an important role.

To better understand the nature of the magnetic and magnetocaloric properties, we have also measured the heat capacity of the $GdFeO_3$ single crystal. At zero field, C_p decreases with the decrease in temperature down to 10 K and then increases with further decrease in temperature and exhibits a prominent λ-like anomaly at around 2.5 K, indicating a paramagnetic-to-AFM transition of the Gd sublattice. To calculate the lattice heat capacity, the zero-field $C_p(T)$ curve in the high-temperature region has been fitted using the Debye model as shown by the solid line in Fig. 6. With the application of field, the peak broadens due to the Schottky effect and shifts toward higher temperature. Qualitatively, similar behavior has been observed in $Gd(HCOO)_3$, which also exhibits large MCE at low temperature [25]. The temperature dependence of C_p for different applied fields is shown in Fig. 7(a). The obtained

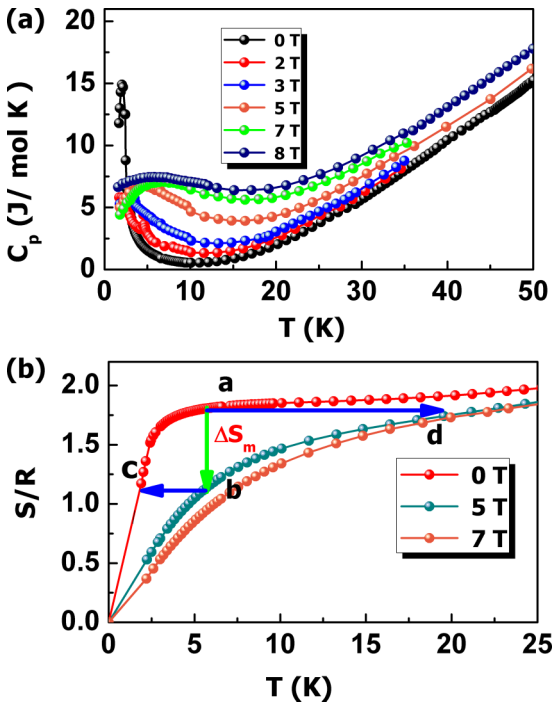

FIG. 7. (a) Temperature dependence of the heat capacity for the $GdFeO_3$ single crystal at different magnetic fields. (b) Temperature dependence of the magnetic entropy for the $GdFeO_3$ single crystal due to the ordering of the Gd sublattice obtained from the heat-capacity data. The vertical arrow shows the isothermal magnetization process for the magnetic field change (0–5 T), whereas the horizontal arrows from **a** to **d** and from **b** to **c** represent cooling and heating effects, respectively, in the adiabatic demagnetization and adiabatic magnetization at 6 K, for a change of 5 T magnetic field as an example.

lattice part was subtracted from the total heat capacity to determine the magnetic contribution (C_m) to the heat capacity and hence the entropy (S) associated with the AFM ordering at 2.5 K. S is obtained by integrating $(C_m/T)dT$ and is shown in Fig. 7(b). At zero field, the estimated saturation value of S is 17.3 J/mol K, which is very close to that expected for Gd^{3+}. It may be further noted that more than 85% of the magnetic entropy is released just below the AFM transition. This suggests that a major fraction of $4f$ spins is taking part in the magnetic ordering. However, the magnetic entropy shifts rapidly toward the higher-temperature side with the application of magnetic field.

To check the consistency of our results on magnetic entropy change estimated from $M(H)$ data, ΔS_m has also been calculated independently from the field dependence of heat capacity using the relation $\Delta S_m = \int_0^T [C_p(H_2,T) - C_p(H_1,T)]/T dT$, where $C_p(H,T)$ is the specific heat at a field H. ΔS_m calculated from the heat capacity data is shown in Fig. 8(a) as a function of temperature. It is clear from the plots that the values of ΔS_m calculated from the magnetization and heat-capacity data are close to each other.

It has already been mentioned that another very important parameter related to the magnetic refrigeration is ΔT_{ad}, which is the isentropic temperature difference between $S(H,T)$ and $S(0,T)$. ΔT_{ad} can be calculated from the zero-field $C_p(T)$ and $\Delta S_m(H,T)$ data. For this, we have calculated the entropy

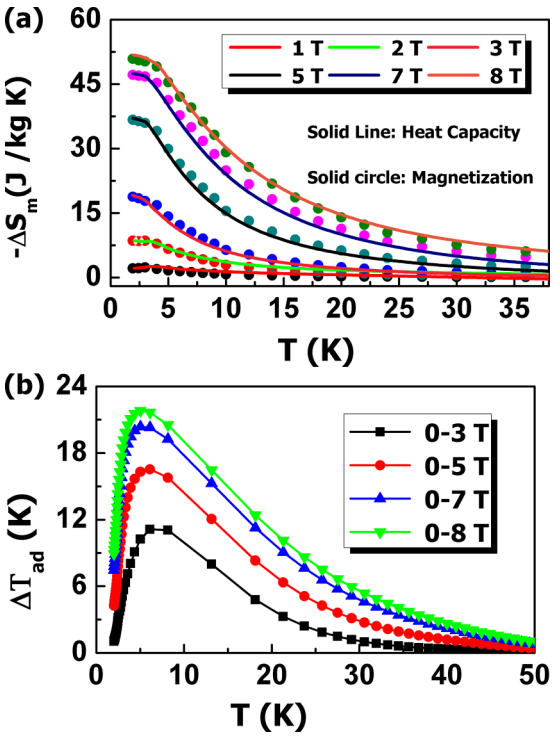

FIG. 8. (a) Comparison between ΔS_m calculated from magnetization and that calculated from heat-capacity data in $GdFeO_3$. (b) Temperature dependence of ΔT_{ad} for the $GdFeO_3$ single crystal.

$S(H,T)$ at field H after subtracting $\Delta S_m(H,T)$ determined using the heat-capacity data, from the zero-field entropy $S(0,T)$. The temperature dependence of ΔT_{ad} is shown in Fig. 8(b). The maximum value of ΔT_{ad} reaches as high as 22 K at 8 T and 5 K. Thus, both ΔS_m and ΔT_{ad} are very large in $GdFeO_3$ orthoferrite. Similar to ΔS_m, ΔT_{ad} is also quite large at low and moderate field strength. We would like to mention that these magnetocaloric parameters have reasonably good values close to 20 K, the boiling point of hydrogen. In this context, it may be noted that undoped and doped $EuTiO_3$, $EuDy_2O_4$, and $GdVO_4$ exhibit a huge MCE at low temperature [28,56–59]. The values of ΔS_m^{max} in these compounds are also comparable to the present system. However, $\Delta S_m(T)$ shows a strong decrease in the low-temperature region. In magnetic refrigeration, ΔS_m per unit volume is important. As the density of the studied material (7.4 g cm^{-3}) is high, the value of ΔS_m per unit volume for $GdFeO_3$ is also quite large.

How much work is done during the reversible thermal changes in the materials themselves is an important parameter for the application purpose [60]. For this, the energy efficiency for the $GdFeO_3$ single crystal has been calculated and compared with other low-temperature magnetic refrigerants. The amount of heat (Q) released during the isothermal process has been deduced using the relation $Q = T_0\Delta S_m$, where T_0 is the operating temperature. We have also estimated the required amount of mechanical work (W_m) or electrical work (W_e) to drive the reversible caloric effects using the method described by Moya *et al.* [60]. As the value of Q is very sensitive to T, we have used $T_0 = 5$ K, around which $\Delta S_m(T)$ exhibits a maximum. Using these parameters, both mechanical efficiency (η_m) and electrical efficiency (η_e) are calculated for the $GdFeO_3$ single crystal and other systems from the reported data. For comparison, η_m and η_e are shown in Table I. It is clear from the table that both η_m and η_e are higher for $GdFeO_3$ as compared to manganites, vanadates, and RR_2O_4-type compounds, which also exhibit large MCE. We have also calculated η_m and η_e at 2 K, i.e., below the liquid helium temperature and at the liquid hydrogen temperature, 20 K. The values of η_m at 2 T are 18.3% and 118% at 2 and 20 K, respectively, and the corresponding values of η_e are 6% and 13%. At low temperature below T_0, Q decreases rapidly due to the decrease of both T and ΔS_m. As ΔS_m for $GdFeO_3$ is almost temperature independent down to 2 K, the decrease in Q is due to the decrease of T only. As a result, its efficiency is expected to be higher compared to other systems.

IV. SUMMARY

In summary, we have studied the magnetic and magnetocaloric properties of a single-crystal $GdFeO_3$ sample through magnetization and heat-capacity measurements. The spin compensation temperature is observed to decrease with field and disappears at around 350 Oe, which is close to the internal magnetic field produced by the Fe^{3+} moments at the Gd^{3+} site. Unlike other orthoferrites, the magnetic properties of $GdFeO_3$ are almost isotropic along different crystallographic axes due to the absence of magnetocrystalline anisotropy. The maximum values of the adiabatic temperature change and isothermal entropy change are as high as 22 K at 8 T and 52.5 J/kg K at 9 T, respectively. The isothermal entropy change calculated from magnetization data for the polycrystalline sample is also very high. This compound also demonstrates a remarkable magnetocaloric effect even at low and intermediate applied fields. Unlike several potential

TABLE I. Comparison of the electrical and mechanical efficiencies of different magnetocaloric materials with respect to $GdFeO_3$ (T_0, operating temperature; ΔH_0, change in applied magnetic field; Q, heat; W, work; efficiency, Q/W). Data for $\Delta H_0 = 5$ T are presented parenthetically.

Material	T_0 (K)	ΔH_0 (T)	Q (J cm^{-3})	Electrical work (J cm^{-3})	Electrical efficiency, η_e (%)	Mechanical work (J cm^{-3})	Mechanical efficiency, η_m (%)	Ref.
$GdFeO_3$	5	2 (5)	0.28 (1.06)	2.04 (12)	14 (9)	0.49 (2.74)	57 (39)	This work
$DyMnO_3$	5	2 (5)	0.03 (0.12)	2.54 (12.31)	1.20 (1)	1.01 (4.8)	3 (2)	[26]
$GdVO_4$	5	2 (5)	0.25 (1.06)	2.13 (12.40)	11 (8)	0.56 (2.60)	44 (40)	[56]
$EuDy_2O_4$	5	2 (5)	0.31 (0.83)	2.83 (14.88)	10 (5)	1.10 (4.10)	30 (20)	[28]
$HoMn_2O_5$	5	2 (5)	0.053 (0.134)	1.18 (11)	3 (1.2)	0.358 (1.8)	15 (7.4)	[27]

magnetic refrigerants with similar transition temperature, ΔS_m in the present compound does not decrease at low temperature. Our result suggests that $GdFeO_3$ could be a potential material for magnetic refrigeration below 40 K.

ACKNOWLEDGMENTS

The authors would like to thank A. Pal for technical help during sample preparation and measurements and N. Khan for his valuable suggestions.

[1] K. A. Gschneidner, Jr., V. K. Pecharsky, and A. O. Tsokol, Rep. Prog. Phys. **68**, 1479 (2005).
[2] O. Gutfleisch, M. A. Willard, E. Bruck, C. H. Chen, S. G. Sankar, and J. P. Liu, Adv. Mater. **23**, 821 (2011).
[3] B. G. Shen, J. R. Sun, F. X. Hu, H. W. Zhang, and Z. H. Cheng, Adv. Mater. **21**, 4545 (2009).
[4] B. F. Yu, Q. Gao, B. Zhang, X. Z. Meng, and Z. Chen, Int. J. Refrig. **26**, 622 (2003).
[5] J. Liu, T. Gottschall, K. P. Skokov, J. D. Moore, and O. Gutfleisch, Nat. Mater. **11**, 620 (2012).
[6] O. Tegus, E. Bruck, K. H. J. Buschow, and F. R. De Boer, Nature (London) **415**, 150 (2002).
[7] M. Foldeaki, R. Chachine, and T. K. Bose, J. Appl. Phys. **77**, 3528 (1995).
[8] V. K. Pecharsky and K. A. Gschneidner, Jr., Phys. Rev. Lett. **78**, 4494 (1997).
[9] V. K. Pecharsky and K. A. Gschneidner, Jr., J. Magn. Magn. Mater. **167**, L179 (1997).
[10] H. Zeng, C. Kuang, and J. Zhang, Bull. Mater. Sci. **34**, 825 (2011).
[11] P. J. von Ranke, V. K. Pecharsky, and K. A. Gschneidner, Jr., Phys. Rev. B **58**, 12110 (1998).
[12] J. C. Patnino and N. A. De Oliveira, Intermetallics **64**, 59 (2015).
[13] L. Li, K. Nishimura, W. D. Hutchison, Z. Qian, D. Huo, and T. Namiki, Appl. Phys. Lett. **100**, 152403 (2012).
[14] A. Rostamnejadi, M. Venkatesan, P. Kameli, H. Salamati, and J. M. D. Coey, J. Magn. Magn. Mater. **323**, 2214 (2011).
[15] M. Baazaoui, M. Boudard, and S. Zemni, Mater. Lett. **65**, 2093 (2011).
[16] R. Mondal, R. Nirmala, J. A. Chelvane, and A. K. Nigam, J. Appl. Phys. **113**, 17A930 (2013).
[17] E. Bruck, O. Tegus, D. T. C. Thanh, and K. H. J. Buschow, J. Magn. Magn. Mater. **310**, 2793 (2007).
[18] H. Wada and Y. Tanabe, Appl. Phys. lett. **79**, 3302 (2001).
[19] E. Bruck, M. Ilyn, A. M. Tishin, and O. Tegus, J. Magn. Magn. Mater. **290**, 8 (2005).
[20] K. Y. Jiao, Z. X. Qun, G. Heng, M. Yue, and C. Z. Hua, Chin. Phys. B **24**, 037501 (2015).
[21] Y. J. Ke, X. Q. Zhang, Y. Ma, and Z. H. Cheng, Sci. Rep. **6**, 19775 (2016).
[22] Y. Cao, M. Xiang, W. Zhao, G. Wang, Z. Feng, B. Kang, A. Stroppa, J. Zhang, W. Ren, and S. Cao, J. Appl. Phys. **119**, 063904 (2016).
[23] R. Huang, S. Cao, W. Ren, S. Zhan, B. Kang, and J. Zhang, Appl. Phys. Lett. **103**, 162412 (2013).
[24] M. Shao, S. Cao, Y. Wang, S. Yuan, B. Kang, and J. Zhang, Solid State Commun. **152**, 947 (2012).
[25] E. K. G. Lorusso, J. W. Sharples, E. Palacios, O. Roubeau, E. K. Brechin, R. Sessoli, A. Rossin, F. Tuna, E. J. L. Mclnnes, D. Collison, and M. Evangelisti, Adv. Mater. **25**, 4653 (2013).
[26] A. Midya, S. N. Das, P. Mandal, S. Pandya, and V. Ganesan, Phys. Rev. B **84**, 235127 (2011).
[27] M. Balli, S. Jandl, P. Fournier, and M. M. Gospodinov, Appl. Phys. Lett. **104**, 232402 (2014).
[28] A. Midya, N. Khan, D. Bhoi, and P. Mandal, Appl. Phys. Lett. **101**, 132415 (2012).
[29] S. J. Yuan, W. Ren, F. Hong, Y. B. Wang, J. C. Zhang, L. Bellaiche, S. X. Cao, and G. Cao, Phys. Rev. B **87**, 184405 (2013).
[30] S. Cao, H. Zhao, B. Kang, J. Zhang, and W. Ren, Sci. Rep. **4**, 5960 (2014).
[31] A. V. Kimel, A. Kirilyuk, A. Tsvetkov, R. V. Pisarev, and T. Rasing, Nature (London) **429**, 850 (2004).
[32] H. J. Zhao, Y. Yang, W. Ren, A. J. Mao, X. M. Chen, and L. Bellaiche, J. Phys.: Condens. Mater. **26**, 472201 (2014).
[33] H. Wu, S. Cao, M. Liu, Y. Cao, B. Kang, J. Zhang, and W. Ren, Phys. Rev. B **90**, 144415 (2014).
[34] Y. Tokunaga, Y. Taguchi, T. Arima, and Y. Tokura, Phys. Rev. Lett. **112**, 037203 (2014).
[35] Y. Tokunaga, N. Furukawa, H. Sakai, Y. Taguchi, T. Arima, and Y. Tokura, Nat. Mater. **8**, 558 (2009).
[36] Y. Tokunaga, S. Iguchi, T. Arima, and Y. Tokura, Phys. Rev. Lett. **101**, 097205 (2008).
[37] S. Geller, J. Chem. Phys. **24**, 1236 (1956).
[38] G. W. Durbin, C. E. Johnson, and M. F. Thomas, J. Phys. C: Solid State Phys. **10**, 1975 (1977).
[39] F. Arfat, Afr. Phys. Rev. **3**, 0006 (2009).
[40] Z. Y. Zhao, X. M. Wang, C. Fan, W. Tao, X. G. Liu, W. P. Ke, F. B. Zhang, X. Zhao, and X. F. Sun, Phys. Rev. B **83**, 014414 (2011).
[41] J. D. Cashion, A. H. Cooke, D. M. Matin, and M. R. Wells, J. Phys. C: Solid State Phys. **3**, 1612 (1970).
[42] M. A. Gilleo, J. Chem. Phys. **24**, 1239 (1956).
[43] H. J. Zhao, L. Bellaiche, X. M. Chen, and J. Iniguez, Nat. Commun. **8**, 14025 (2017).
[44] F. Pomiro, R. D. Sanchez, G. Cuello, A. Maignan, C. Martin, and R. E. Carbonio, Phys. Rev. B **94**, 134402 (2016).
[45] A. Kumar and S. M. Yusuf, Phys. Rep. **556**, 1 (2015).
[46] T. Bora and S. Ravi, J. Appl. Phys. **114**, 033906 (2013).
[47] O. V. Billori, F. Pomiro, S. A. Cannas, C. Martin, A. Maignan, and R. E. Carbonio, J. Phys.: Condens. Matter **28**, 476003 (2016).
[48] P. Gupta and P. Poddar, Inorg. Chem. **54**, 9509 (2015).
[49] A. H. Cooke, D. M. Matin, and M. R. Wells, J. Phys. C: Solid State Phys. **7**, 3133 (1974).
[50] R. Skomki and D. J. Sellmyer, J. Rare Earth **27**, 4 (2009).
[51] G. Gorodetsky and D. Treves, Phys. Rev. **135**, A97 (1964).
[52] R. L. White, J. Appl. Phys. **40**, 1061 (1969).
[53] F. J. Morin, Phys. Rev. **78**, 819 (1950).
[54] Z. Y. Zhao, X. Zhao, H. D. Zhou, F. B. Zhang, Q. J. Li, C. Fan, X. F. Sun, and X. G. Li, Phys. Rev. B **89**, 224405 (2014).

[55] A. Midya and P. Mandal, J. Appl. Phys. **116**, 223905 (2014).
[56] K. Dey, A. Indra, S. Majumdar, and S. Giri, J. Mater. Chem. C **5**, 1646 (2017).
[57] A. Midya, P. Mandal, K. Rubi, R. Chen, J. S. Wang, R. Mahendiran, G. Lorusso, and M. Evangelisti, Phys. Rev. B **93**, 094422 (2016).
[58] S. Roy, N. Khan, and P. Mandal, Appl. Mater. **4**, 026102 (2016).
[59] Km. Rubi, P. Kumar, D. V. M. Repaka, R. Chen, J. S. Wang, and R. Mahendiran, Appl. Phys. Lett. **104**, 032407 (2014).
[60] X. Moya, E. Defay, V. Heine, and N. D. Mathur, Nat. Phys. **11**, 202 (2015).